Available online at www.sciencedirect.com
ScienceDirect
Journal of Catalysis 245 (2007) 285–300
JOURNAL OF CATALYSIS
www.elsevier.com/locate/jcat

Methylation of phenol over high-silica beta zeolite: Effect of zeolite acidity and crystal size on catalyst behaviour

M. Bregolato [a], V. Bolis [b], C. Busco [b], P. Ugliengo [c], S. Bordiga [c], F. Cavani [d], N. Ballarini [d], L. Maselli [d], S. Passeri [d], I. Rossetti [a], L. Forni [a,*]

[a] *Dipartimento Chimica Fisica ed Elettrochimica, Università di Milano, via C. Golgi 19, I-20133 Milano, and INSTM, Research Unit of Milano, Italy*
[b] *Dipartimento DiSCAFF, Università del Piemonte Orientale "A. Avogadro", via G. Bovio 6, I-28100 Novara, and INSTM, Research Unit of Piemonte Orientale and NIS Centre of Excellence, Italy*
[c] *Dipartimento Chimica IFM, Università di Torino, via P. Giuria 7, I-10125 Torino, and INSTM, Research Unit of Torino and NIS Centre of Excellence, Italy*
[d] *Dipartimento Chimica Industriale e dei Materiali, Università di Bologna, v.le Risorgimento 4, I-40136 Bologna, and INSTM, Research Unit of Bologna, Italy* [1]

Received 10 May 2006; revised 20 October 2006; accepted 21 October 2006

Available online 28 November 2006

Abstract

A systematic investigation was carried out to elucidate several aspects of the gas/solid methylation of phenol over high Si/Al ratio beta-structured zeolite in protonated form, characterised by various techniques, including XRD, SEM, BET, ICP, FTIR, TGA, microcalorimetry, and modeling by ab initio calculations. Data on the characteristics and the kinetic and mechanistic features of the catalytic reaction, as well as on catalyst deactivation, show that these zeolites, besides being very active for the present reaction, lead to cresols and anisole as primary products. As catalyst deactivation proceeds, the selectivity to cresols and anisole increases substantially, accompanied by a rapid decrease in selectivity to polyalkylated species. Medium- to low-strength silanols are the main contributors to catalyst surface acidity. High-strength Lewis acid sites either are virtually absent (especially when metal cations partially substitute for protons) or play a role essentially in catalyst deactivation. Stacking faults in the zeolite framework, generated by the intergrowth of at least two beta polymorphs, lead to an increased concentration of silanol-based Brønsted acid sites. Deactivation is due to the interaction of phenol and oxygenated products with the silanol-based acid sites and of methanol only with the strong acid sites of both Lewis and Brønsted nature. Self-oligomerisation–cyclisation of methanol to olefins and aromatics, followed by further alkylation to aromatic C atoms, contributes to catalyst deactivation. At any conversion level and at any temperature, the anisole/cresol ratio is systematically lower for the larger-crystal size zeolite, because the secondary transformations of anisole to cresols by both intramolecular rearrangement and intermolecular alkylation of phenol is favoured by the longer residence time of anisole within the zeolite pores.

Keywords: Methylation of phenol; Zeolite beta; Crystal size; Surface acidity; FTIR; Microcalorimetry; Ab initio modeling; Catalyst activity and deactivation

1. Introduction

Methylation of phenol over acidic catalysts represents an industrially interesting process by which a set of important chemicals and chemical intermediates, such as cresols, anisole, and polyalkylated phenols, can be prepared [1]. The most widely investigated catalysts include strong Brønsted-type acid materials, such as H-Y and H-ZSM-5 zeolites [2–13], as well as weaker acid catalysts, such as metal phosphates [14,15]. The main limit of zeolites is the low selectivity achieved to one specific compound, because several products are obtained (*O*-alkylated, mono- and poly-*C*-alkylated), the selectivity of which is a function of phenol conversion, reaction conditions, and zeolite characteristics. This is not the case for heterogeneous basic-catalysed methylation, a much more specific reaction. In fact, this reaction yields almost exclusively the products of ortho-*C*-alkylation [16–20].

Furthermore, alkylation reactions over solid acid catalysts, especially with reactants in the gas phase, are usually accompanied by several unwanted side reactions, triggered by the same

* Corresponding author. Fax: +39 02 50314300.
E-mail address: lucio.forni@unimi.it (L. Forni).
[1] A Partner of Idecat NoE, 6FP of the EU.

0021-9517/$ – see front matter
doi:10.1016/j.jcat.2006.10.024

surface acidity of the catalyst, leading to a more or less rapid deactivation of the catalyst due to fouling by carbonaceous deposits, usually referred to as "coke" [21]. However, it is worth noting that, to the best of our knowledge, the scientific literature on the alkylation with alcohols of phenol and of phenol derivatives, especially from a reaction kinetics standpoint, does not explicitly take any catalyst deactivation effect into consideration.

The literature on gas-phase alkylation of phenol with alcohols over beta zeolites is scarce [22–27]. Over beta zeolite, a somewhat different acidity can add to that based on Al^{3+} sites. Indeed, in such a zeolite, randomly intergrown structures of two or even three different polymorphs, with a considerable amount of random stacking faults, leads to a substantial increase in lattice defects and structural disorder [28]. This disorder creates additional internal surface hydroxylated species (SiOH nests of variable geometrical arrangement) and Lewis-type electron acceptor sites. Consequently, both catalyst activity and resistance to coking are simultaneously affected by zeolite crystal structure and pore width, nature and concentration of surface acid sites, and zeolite crystal size [29–31].

The aim of the present work was to investigate the effect on catalytic performance for phenol methylation of properly prepared samples of H-beta zeolite of similar Si/Al ratio but much different crystal size. In fact, it is expected that in a complex reaction pattern, including parallel and consecutive reactions, the distribution of products can be greatly affected by the intraparticle residence time of products. Besides reaction rate and selectivity to the various products, the present analysis takes into account the activity decay and the change of selectivity with time on stream, looking for correlations between catalytic behaviour and the zeolites' physicochemical characteristics.

2. Experimental

2.1. Catalyst preparation

Three main samples of beta zeolite, designated beta-1, beta-2, and beta-3 (Table 1), were prepared by hydrothermal synthesis [32,33]. Tetraethyl-orthosilicate (TEOS, 98% pure, Aldrich), tetraethylammonium hydroxide (TEAOH, 40% aqueous solution, Fluka), sodium aluminate (56% Al_2O_3, 37% Na_2O, Carlo Erba), and NaOH (97% pure, Aldrich) were used as reagents. The silico-aluminate precursor gel was obtained by vigorously stirring the mixture of reagents at room temperature for several hours. After hydrolysis of the organo-silicon compound was complete, stirring was continued for at least 24 h under final gentle warming, to remove the ethanol that was released.

The synthesis of the zeolite was then carried out at 135 °C (for beta-1) or 150 °C (for beta-2 and beta-3) in PTFE-lined stainless steel autoclaves, tumbling at 20 rpm. After 24 h for beta-1, 48 h for beta-2, and 94 h for beta-3, the autoclaves were rapidly cooled, and the solid was recovered from the milky suspension by centrifugation at 40,000g. The solid was then repeatedly washed with distilled water until the washing liquid was neutral, dried at 120 °C overnight, and calcined in nitrogen and air flow up to 550 °C, to remove the TEAOH trapped in the channels of the zeolite crystals. The as-prepared samples then underwent three ion exchanges for 3 h at 80 °C with fresh 0.1 M ammonium nitrate (Janssen, "pro analysi") solution. After the final exchange, the solid was separated by centrifugation, repeatedly washed with distilled water, and calcined in air at 550 °C to obtain the final protonated zeolite by decomposition of ammonium ions.

A fourth sample (beta-silicalite, with an Si/Al ratio >500) was also prepared for characterisation comparison purposes only. This involved preparing a special templating agent, 4,4′-trimethylene-bis(N-benzyl-N-methyl-piperidinium)-dihydroxide; the commonly used TEAOH failed to lead to the desired beta structure for very high Si/Al ratios [34].

The template solution was prepared as follows. First, 77 g of 4,4′-trimethylene-bis-(1-methyl-piperidine) (Aldrich, 98+% pure) was dissolved in 103 g of ethanol (Fluka, anhydrous). To this solution was added 110 g of benzyl bromide (Fluka, 98% pure) dropwise under vigorous stirring. The solid dibromide precipitate so formed was repeatedly washed with anhydrous ethanol and dried under flowing nitrogen. The dihydroxide was then obtained from the dibromide by electrodialysis, using an electrolytic cell equipped with an anionic membrane separating the cathodic 0.46 M bromide solution from the anodic 25 wt% aqueous ammonia solution. The final 0.79 M solution of the templating agent was finally obtained by low-temperature removal of excess water.

The synthesis of beta-silicalite was then carried out as described previously, in the absence of sodium aluminate and by substituting the 4,4′-trimethylene-bis(N-benzyl-N-methyl-piperidinium)-dihydroxide for TEAOH. A fifth sample, designed beta-10 and used for comparison purposes only, was kindly supplied by Polimeri Europa srl.

2.2. Catalyst characterisation

The crystalline structure was identified by X-ray diffraction (XRD) using a Philips PW 1820 powder diffractometer,

Table 1
Main characteristics and energetics of interaction with H_2O and CH_3OH of the investigated catalysts

Catalyst	SiO_2/Al_2O_3 mol ratio	Si/Al mol ratio	Al/uc	Av. cryst. size (nm)	SSA (m^2/g)	V_{pTOT} (cm^3/g)	V_{pMicr} (cm^3/g)	Na^+ (wt%)	q_0 H_2O (kJ/mol)	q_0 CH_3OH (kJ/mol)
Beta-1	65	130	≈0.5	200	481	0.343	0.239	2.42	100	–
Beta-2	77	154	≈0.4	100	559	0.627	0.266	0.07	160	50
Beta-3	65	130	≈0.5	590	565	0.324	0.299	0.01	160	50
Beta-silicalite	255	510	<0.1	450	529	0.311	0.270	<0.001	80	–
Beta-10	4.9	9.8	≈6	50	360	–	–	–	165	–

operated at 40 kV and 40 mA, with Ni-filtered Cu$K\alpha$ radiation ($\lambda = 1.5418$ Å). The BET specific surface area (SSA) was measured by N_2 adsorption–desorption at liquid nitrogen temperature on a Micromeritics ASAP 2010 instrument. Zeolite crystal size and shape were determined by scanning electron microscopy (SEM) using either a Cambridge Stereoscan 150 or a Leica LEO 1430 instrument. Elemental analysis was performed on a Varian Liberty 200 inductively coupled plasma (ICP) spectrometer.

Catalyst surface acidity was measured by FTIR spectroscopy using a Perkin-Elmer 1750 spectrometer. First, self-supporting wafers of pure zeolite were evacuated at 500 °C in vacuo (residual $p = 10^{-6}$ mbar). Then adsorption of pyridine was carried out at room temperature, followed by desorption carried out by outgassing the sample at 50, 150, 250, 350, and 450 °C. The FTIR spectrum was recorded after evacuation at each temperature level.

The reactivity toward CH_3OH, the large-excess reactant of the methylation reaction (vide infra), was also investigated by IR. The interaction between CH_3OH and beta-1, beta-2, and beta-3 catalysts, after preactivation in vacuo (residual $p = 10^{-5}$ Torr) at 773 K, was analysed at 2 cm^{-1} resolution on a Bruker IFS 66 FTIR spectrometer, equipped with an MCT detector. The samples were preevacuated as for the acidity measures (vide supra).

The catalysts' adsorption features were investigated by contacting (at 303 K) the activated samples with CH_3OH vapour, as well as with H_2O vapour, to investigate the hydrophilic/hydrophobic properties of the catalysts. The study was performed using a heat-flow microcalorimeter Tian-Calvet type (C80 by Sétaram) connected to a high-vacuum gas-volumetric glass apparatus, equipped with a Varian Ceramicell 0- to 100-Torr transducer gauge, following a well-established procedure [35–37]. All samples were activated in vacuo for 2 h at a residual pressure $p \leqslant 10^{-5}$ Torr at $T = 873$ K for H-beta and at $T = 673$ K for the all-silica zeolite. The individual activation temperature was selected according to the indications of IR spectroscopy (spectra not reported for brevity), so to achieve the maximum dehydration of the surface compatible with the stability of the structure and aiming for the maximum density of Lewis and Brønsted acidic sites. CH_3OH and H_2O were distilled in vacuo and outgassed by several freeze–pump–thaw cycles. The adsorption measurements have been performed at least twice on a virgin portion of the same batch of the materials, activated under the same conditions, to check the reproducibility of the experiments.

At last, a calculation was made relative to the interaction of CH_3OH and H_2O molecules with a molecular cluster simulating a coordinatively unsaturated framework Al(III) site acting as Lewis (L) acidic site. All calculations have been run at ab initio level using the B3-LYP/6-31 + G(d,p) model chemistry [38]. The binding energies (BEs) of the probe molecules with the L site were calculated and compared with the enthalpy change associated to the adsorption processes on the real systems.

2.3. Catalytic activity tests

Methylation of phenol was carried out in a continuous-downflow tubular reactor at four different temperatures, ranging from 320 to 450 °C, at atmospheric total pressure. An excess of methanol with respect to the stoichiometric requirement for the methylation of phenol was fed (methanol/phenol feed ratio = 7/1). In fact, due to the strong interaction between phenol and the catalyst, acceptable reaction rates are obtained only when the partial pressure of methanol is much higher than that of phenol. Usually methanol/phenol feeding ratios >5 are used [39] for an analysis of the effect of such a ratio on catalytic performance, to obtain a phenol conversion >10–20% at $T < 400$ °C. On the other hand, feeding ratios >10 favour the formation of polyalkylated phenols. Our aim was to investigate the selectivity ratio between O- and C-alkylated compounds, with minimal formation of polyalkylated products. Therefore, we chose a methanol/phenol molar ratio of 7/1 as a compromise between these two counteracting effects.

Catalyst samples of 0.6 g were loaded. The flow rate of the reactants was 60 cm^3/min of gaseous N_2 and 1.75×10^{-3} cm^3/min of organic liquid feeding mixture, so as to have a residence time value of $\tau = 0.98$ s ($cm^3_{\text{catalyst bed}}$ s/$cm^3_{\text{overall gaseous feeding flow}}$). The reactor temperature was maintained at the desired value by an electric furnace surrounding the reactor and governed by a TRC, through a thermocouple placed within the catalyst bed. Reactor effluent analysis was made by means of a Thermo Focus gas chromatograph, equipped with a HP-5 semicapillary column.

When needed, the catalyst was regenerated in situ in flowing air (20 cm^3/min) by increasing the temperature by 5 °C/min from room temperature up to 300 °C, then by 0.83 °C/min up to 350, 400, and 450 °C. After each temperature step (i.e., 300, 350, 400, and 450 °C) temperature was kept constant for 1 h.

2.4. Coke analysis

Samples of aged catalyst, recovered after a few hours on stream at 390 °C, were analysed according to a well-known technique [40] to collect information on the amount and nature of the fouling carbonaceous material (coke). A weighed portion of aged catalyst was disaggregated in HF (40% aqueous solution) to dissolve the zeolite and allow collection of the remaining carbonaceous solid particles by filtration and drying. The carbonaceous solid particles were repeatedly leached with small portions of fresh CH_2Cl_2 and then dried and weighed. The leaching CH_2Cl_2 solutions were combined, and most of the solvent was removed in vacuo at room temperature. The concentrated solution of the soluble coke was then analysed by gas chromatography-quadrupolar mass spectrometry (GC-QMS) by an Agilent HP 5973N GC-MS instrument.

For the beta-1 and beta-2 aged samples only, the amount of accumulated carbonaceous matter was also evaluated by thermogravimetry in air using a TA TGA 2050 instrument. The following heating program was followed: 80 °C in flowing N_2 for 5 min, heating from 80 to 550 °C (5°/min) in 60 ml/min flowing air, and a final isothermal step at 550 °C for 60 min.

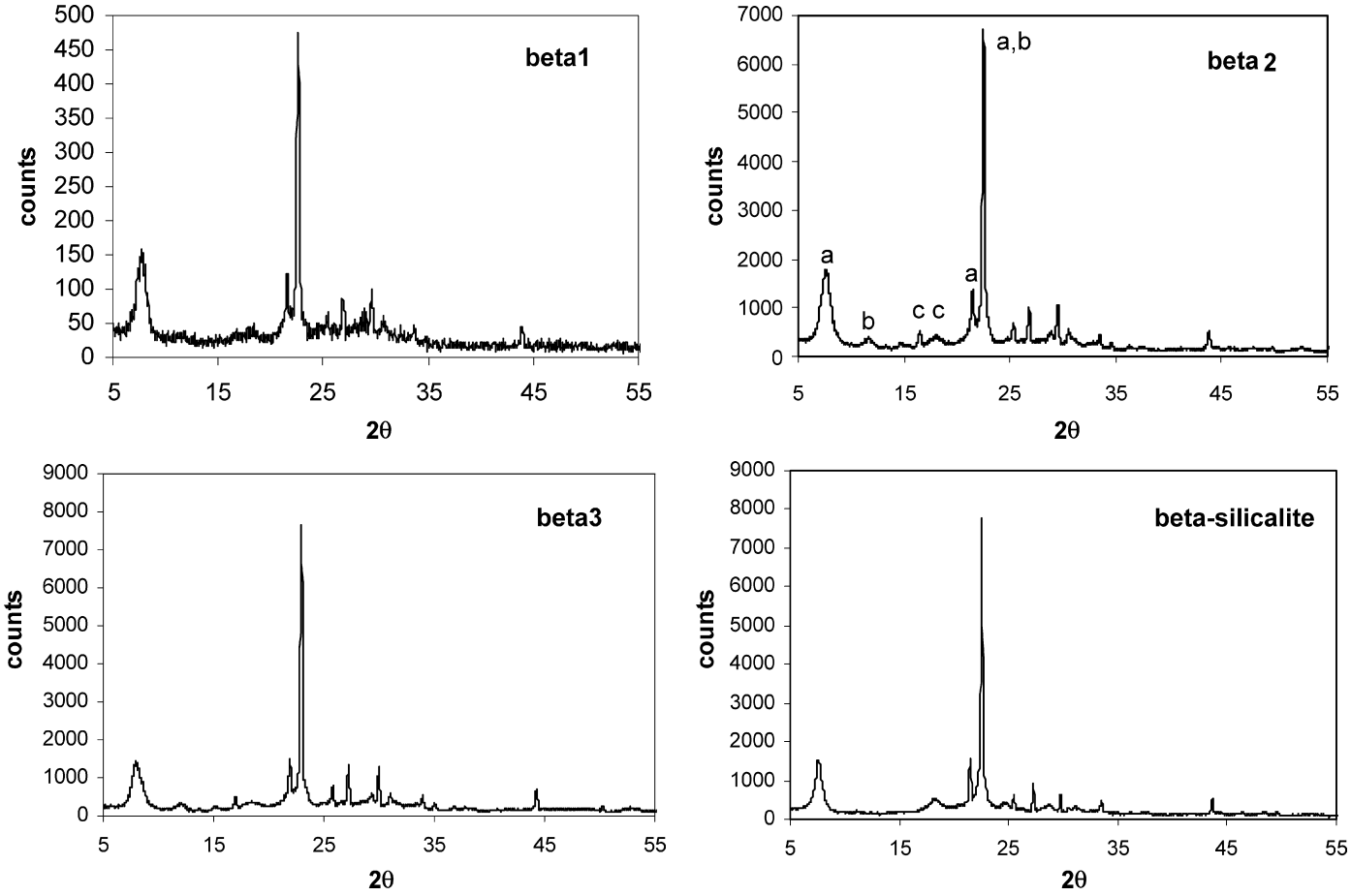

Fig. 1. XRD patterns of the catalysts prepared. (a), (b), and (c) refer to polymorphs A, B and C [42,43].

3. Results and discussion

3.1. Catalysts characterisation

3.1.1. Surface area, crystal size, and Si/Al ratio

Under the synthesis conditions adopted, beta zeolite was the only crystalline phase obtained. The XRD patterns matched those reported in the literature [41–43]. Beta-1 had less crystalline than the other samples (Fig. 1). Our BETA samples resulted from the intergrowth of two polymorphs, A and B [43], or even of a third polymorph, C [42]. Although our XRD patterns does not allow a reliable quantitative determination of the polymorph distribution, the crystallinity of our samples can be characterised (Table 1) by comparing micropore volume (V_{pMicr}, determined from t-plot data) with total pore volume (V_{pTOT}, determined from the total gas volume adsorbed at saturation).

SSA ranged from 480 to 570 m^2/g (Table 1), typical values for these zeolites. SEM micrographs (Figs. 2a, 2b, and 2d) showed that beta-1, beta-2, and beta-silicalite were composed of spheroidal-shaped crystals with a narrow crystal size distribution. The beta-3 crystals appeared slightly cuboidal-shaped (Fig. 2c). The average particle size, determined by direct measurement on properly enlarged micrographs for the various zeolites, is given in Table 1.

ICP analysis showed a similar SiO_2/Al_2O_3 molar ratio (Table 1) for all samples except, of course, the beta-silicalite. Furthermore, the protonated beta-2 and beta-3 (and mainly beta-silicalite) catalysts were almost Na-free, whereas the beta-1 sample contained a considerable amount of exchangeable Na^+ ions (Table 1).

3.1.2. Reactivity toward CH_3OH from FTIR spectroscopy

All our catalysts, except beta-10, are characterised by a very low Al content (Table 1). This, accompanied by the high structural defectivity (vide supra) of these zeolites, which is associated with a large abundance of silanols, becomes relevant in the spectroscopic features of their reactivity with CH_3OH. Another important point is the concentration of residual Na^+ species, which was rather abundant only in the beta-1 sample (2.42 wt%; Table 1).

After activation at 773 K, all samples (Fig. 3a) showed no IR bands over 3750 cm^{-1}, characteristic of the hydroxyl groups bound to extra-framework Al (EFA), and all samples exhibited a strong maximum at 3740 cm^{-1}, due to nearly isolated silanols. Another common characteristic was the broad tail at lower frequency, extending up to 3400 cm^{-1}, indicating the presence of an abundant fraction of interacting hydroxyls. No further specific absorption was evident in the beta-1 sample: in particular, no bands were seen in the region where bridging OH groups would be expected. This observation is in agreement

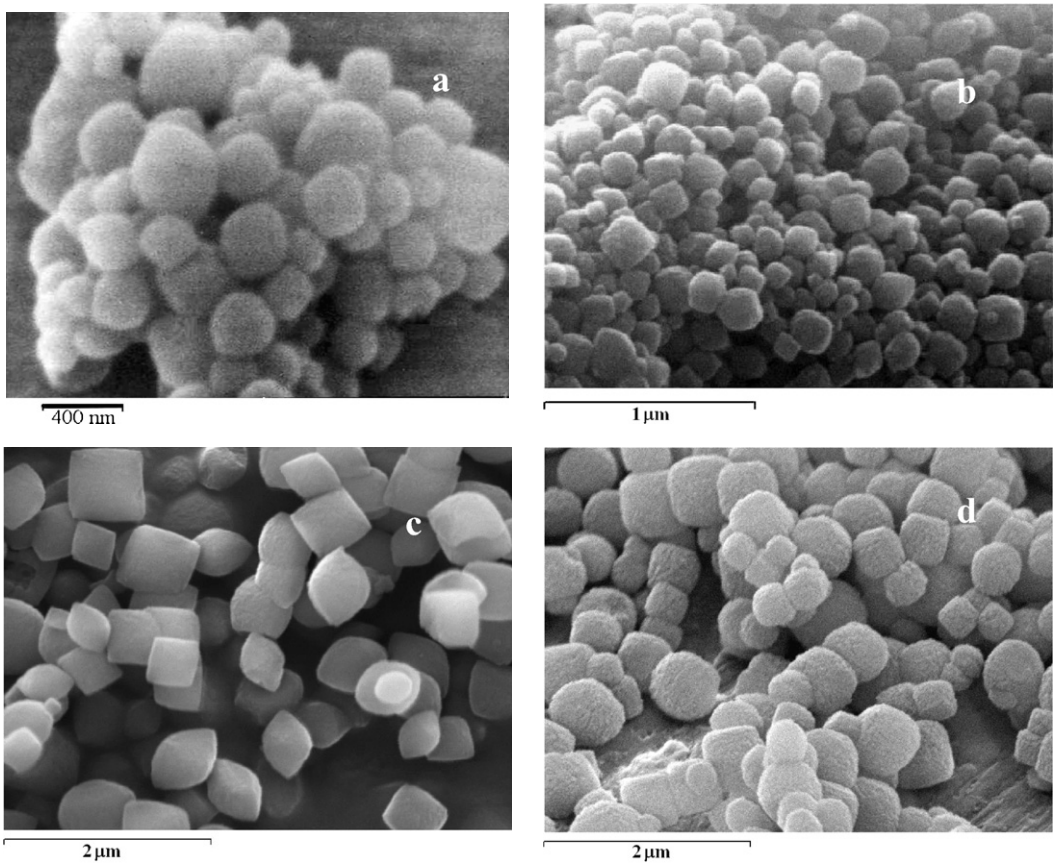

Fig. 2. SEM micrographs of: (a) beta-1, (b) beta-2, (c) beta-3, and (d) beta-silicalite.

with the fact that the beta-1 sample had mainly Na^+ as counterions. The beta-2 sample was characterised by a broad-tailed signal, extending from 3740 to 3400 cm^{-1}, due to H-bound silanols. A second weak maximum was observed at 3580 cm^{-1}, where the band due to bridged B groups (3615 cm^{-1}) is superimposed. The situation is very similar to that observed in beta-3 sample, that shows an even more complex shape of the band in the OH stretching region: peak at 3613 cm^{-1} superimposed to the broad component due to H-bonded silanols (maximum at 3500 cm^{-1}). Also in this case an evaluation of the concentration of bridged B groups is prevented by the mixing with the silanols components.

Fig. 3b shows the reactivity towards CH_3OH of beta 2 and 3. The data on the Na-rich sample, beta-1, are not reported because they did not show any feature associable with bridging Brønsted acid sites. In particular, after interaction with methanol no specific signals ascribable to strong acid sites was noticed (total absence of A, B and C signals, vide infra). In addition, a considerable reversibility of the interaction of beta-1 with methanol was observed, a behaviour typical of purely siliceous materials. This is very likely due to the saturation by Na^+ ions of the strongest acid sites generated by the framework Al ions.

As demonstrated by Pazè et al. [44], in the presence of molecules like H_2O or CH_3OH with medium to high proton affinity, a zeolite, which is characterised by the presence of high Brønsted acidity, is able to realize a strong H-bond interaction, which produces two main effects: at first the band associated to the OH stretching mode is strongly red-shifted, generating an intense and broad absorption which can be extended until 1000 cm^{-1}, while the band due to the overtone of the bending mode of the same species is deeply blue-shifted. From a theoretical point of view, the phenomenon is called Fermi resonance and the effect on the spectra is the appearance of three bands identified as A, B and C, separated by two Evan's windows: the presence and the relative intensity of these three bands indicate the entity of the interaction and consequently the acidity of the material [44–48].

Coming to the effect of increasing dosages of methanol on beta-2 sample (upper left of Fig. 3b), one may observe the progressive erosion of the OH bands and the growth of a very broad absorption with a maximum centred at about 3400 cm^{-1}. This absorption extends till the region of framework vibration, suggesting the presence of some species strongly engaged by methanol. However, because these species are only a minor feature with respect to silanols (characterised by a medium- to low-strength acidity), we did not clearly observe the formation of the A, B, and C components. At around 3000 cm^{-1}, the C–H stretching vibrations of CH_3OH are superimposed. In particular, the absorptions at 3000 and 2958 cm^{-1} represent asymmetric vibrations, whereas the absorption at 2854 cm^{-1} is associated with symmetric modes of the CH_3 groups. The frequencies are shifted upward slightly compared with the vibrations of the free molecules. The band at 2916 cm^{-1} is probably

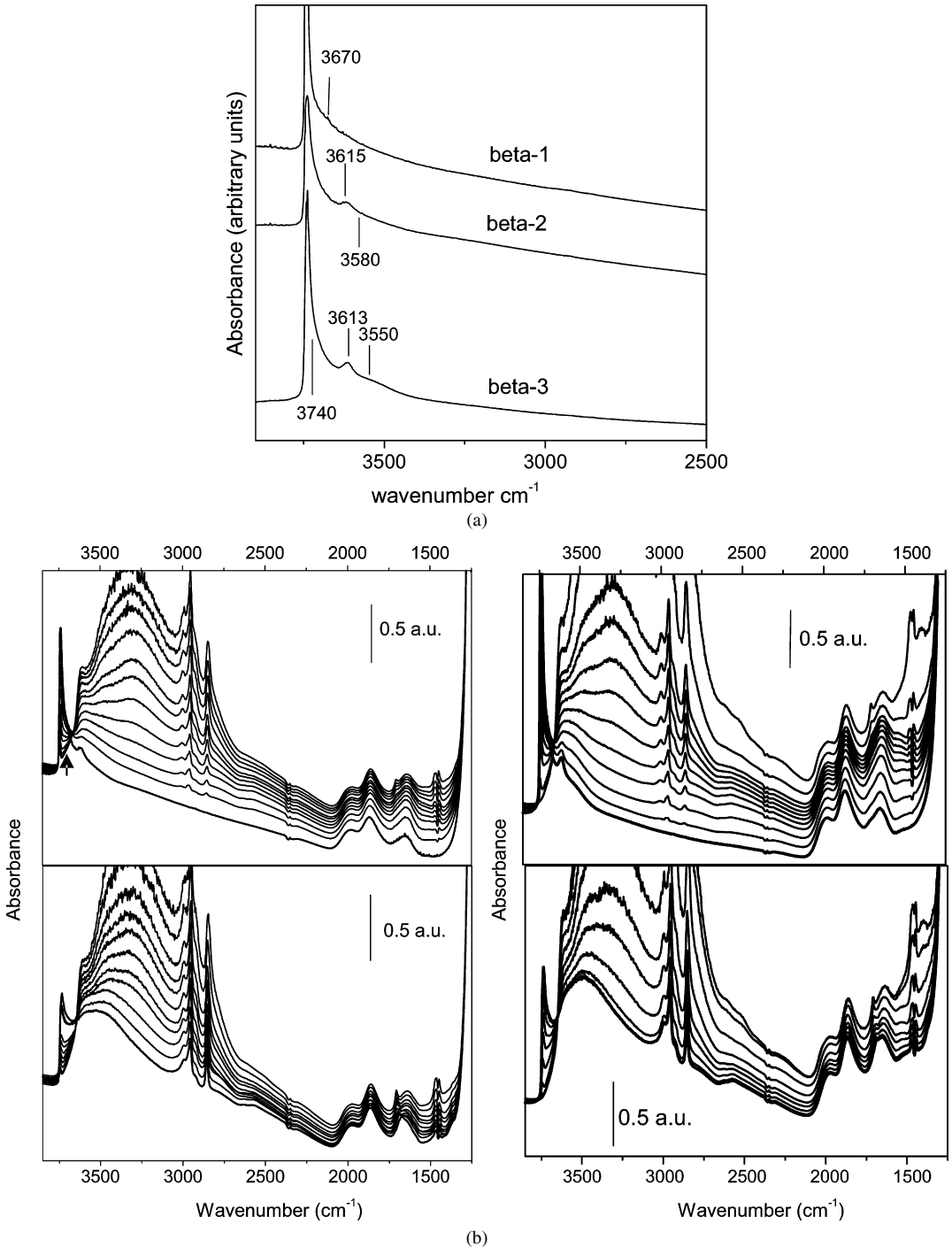

Fig. 3. (a) IR spectra of beta-1, beta-2 and beta-3 zeolites outgassed at 753 K. (b) IR spectra of beta-2 and beta-3 zeolites (left and right couple of figures, respectively). Effect of the interaction with CH_3OH. Top parts of the figure (b) report data related to increasing amounts of methanol; bottom parts of the figure (b) report the effect of progressive pumping out at room temperature.

due to overtones of the $\nu(CH_3)$ bending mode at 1450 cm^{-1}, enhanced by a Fermi resonance effect [49].

The interaction with methanol was not completely reversible on beta-2, as evidenced by the lower-left of Fig. 3b. In particular, only part of the external silanols was restored, whereas the majority of the OH groups remained unaffected by prolonged outgassing at room temperature. The fact that methanol remained entrapped within the zeolite cavities was also demonstrated by the permanent nature of the bands associated with the C–H vibration modes at around 3000 cm^{-1}.

Turning to the data related to the beta-3 sample (upper right of Fig. 3b), at low methanol loadings, the ABC triad, caused by Fermi resonance of the ν stretching and 2δ and 2γ overtones of bond 1 (Scheme 1), can be distinguished.

This in turn induces the formation of two Evans windows, one at about 2720 cm^{-1} and the other at 2000 cm^{-1}. The

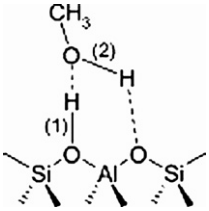

Scheme 1.

Table 2
Summary of the most important IR spectroscopic features

IR feature	Frequency (cm^{-1})		
	Beta-1	Beta-2	Beta-3
ν(OH) isolated silanols	3740	3740	3740
ν(OH) internal and/or H-bonded silanols	3670	3580	3500
ν(OH) SiOHAl	Not visible	3615	3613
ν(OH)···OH–CH_3	Not reported	3400	2100
A_{comp} maximum	Not reported	Not revealed	2900
First Evans window	Not reported	Not revealed	2720
B_{comp} maximum	Not reported	Not revealed	2500
Second Evans window	Not reported	Not revealed	2000
C_{comp} maximum	Not reported	Not revealed	1600

approximate frequency of the ν(OH) mode of ($_{zeolite}$O–H···$O_{methanol}$) in the absence of Fermi resonance effects can be estimated as 2100 cm^{-1}. The corresponding vibration mode of bond 2 (see Scheme 1) is assigned to a component growing at 3500 cm^{-1}. This band grows in parallel with the ABC triplet and confirms the formation of a neutral adduct. The evolution of the spectra in the 2000–1300 cm^{-1} range, where the C component is growing, shows greater complexity. Negative components originate from perturbative effects on the zeolitic framework, inferred by CH_3OH. Moreover, an additional negative band at 1450 cm^{-1} corresponds to an Evans window due to the superposition of the C component with the $\delta(CH_3)$ mode.

At high methanol coverage, the spectra are dominated by an unstructured broad band extending over the entire medium IR region, overshadowing the ABC components associated with formation of the methanol–silanol adducts.

Also with beta-3, the interaction with methanol is only partially reversible, as evidenced by the effect of prolonged outgassing at room temperature (Fig. 3b, lower right). The final spectrum collected (bold curve) is very similar to that obtained for the beta-2 sample.

It may be concluded that the present materials have a low concentration of structural ($SiOH^-Al^+$) strong Brønsted acid sites, and that most of the surface acidity comes from relatively weaker (SiOH nests) Brønsted silanol species. At reaction temperature, the slightly higher abundance of strong acidic sites present in the beta-3 sample could have only a minor effect on overall catalytic activity. This acidity distribution can be considered a major cause of the relatively lower deactivation rate of high-silica BETA zeolite. Table 2 summarizes the most important IR spectroscopic features of our samples.

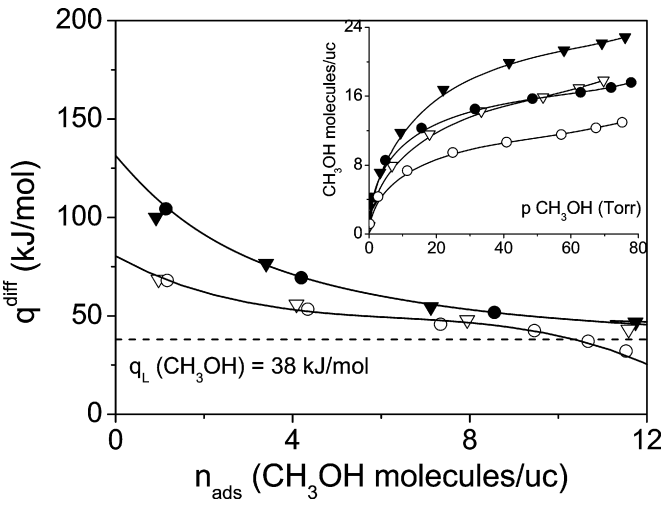

Fig. 4. Differential heats of adsorption of CH_3OH_{vap} on beta-2 (●) and beta-3 (▼) zeolites as a function of the increasing coverage (q^{diff} vs n_{ads}). Inset: volumetric isotherms, n_{ads} (CH_3OH molecules/uc) vs p_{CH_3OH} equilibrium pressure. Solid symbols: ads. I, open symbols: ads. II. $T_{ads} = 303$ K.

3.1.3. Energetics and hydrophilicity/hydrophobicity of active sites

As mentioned earlier, the energetics of adsorption and hydrophilic/hydrophobic properties of the present catalysts were investigated by progressive adsorption of CH_3OH and water vapour, monitored by microcalorimetry. The integral heat evolved (Q^{int}), as well as the adsorbed amount (n_{ads}) for small adsorptive increments, were determined in the same experiment, as described previously [35–37]. The reversibility/irreversibility on evacuation of first-run-adsorbed phase (ads. I) at room temperature was checked by performing a second adsorption run (ads. II) after outgassing the sample overnight (residual $p \leqslant 10^{-5}$ Torr). The adsorbed amounts ($n_{ads} = CH_3OH$ or H_2O molecules per unit cell) were collected as volumetric isotherms. Calorimetric data were collected either as differential heats of adsorption ($q^{diff} = \delta Q^{int}/\delta n_{ads}$) or as integral molar heats of adsorption $[q^{mol}]_p = (Q^{int}/n_{ads})_p$. The $[q^{mol}]_p$ quantities are intrinsically average values, referring to the thermal response of the surface as a whole from the beginning of the adsorption process up to the equilibrium pressure, whereas the q^{diff} quantities represent a reasonable measure of the energy of interaction of the probe molecule with the individual sites at any adsorbate coverage.

Fig. 4 shows the results for beta-2 and beta-3 samples using CH_3OH as a probe. The q^{diff} versus n_{ads} plots give a detailed description of the surface heterogeneity. In particular, the differential heat of adsorption, extrapolated to vanishing coverage (q_0, kJ/mol; Table 1), represents the enthalpy change associated with the adsorption on the most energetic sites. Values of the same order of magnitude were obtained for the binding energy (BE, kJ/mol) through the ab initio calculations (vide infra) for the individual molecular probe's interaction with the model Lewis acid site and corrected for the basis set superposition error by the standard Boys–Bernardi counterpoise method [50].

Inspecting Fig. 4 reveals the following findings:

(i) The q^{diff} versus n_{ads} experimental points of both beta-2 and beta-3 zeolites are best fitted by the same curve, indicating that no significant difference in the acid strength of the two catalysts is demonstrated by the room-temperature adsorption of CH_3OH. The curve starts at $q_0 \sim 130$ kJ/mol and drops down quite smoothly, eventually approaching the latent heat of liquefaction of CH_3OH (38 kJ/mol) at a coverage corresponding to ca. 12 molecules adsorbed per unit cell.

(ii) The only detectable differences between the two catalysts is that the CH_3OH adsorption capacity is significantly larger for beta-3 (see the inset of Fig. 4), because the number of molecules adsorbed per unit cell at any equilibrium pressure investigated is greater than that for beta-2. We ascribe this difference to the different Si/Al ratios, with a slightly higher Al content for beta-3 than for beta-2 [although the two values of Si/Al ratio are too close (130 for the former vs 154 for the latter; Table 1) to permit a more detailed comparison].

(iii) The irreversibly adsorbed CH_3OH, evaluated by the difference between the ads. I and ads. II curves (the latter drawn after outgassing overnight the reversibly adsorbed alcohol of ads. I), amounted to ca. 20% of the total amount adsorbed by both zeolites. Nonetheless, the q^{diff} versus n_{ads} experimental points for the second run were best fitted by the same curve, indicating that for reversible adsorption, a significant difference between the two catalysts is not found when using CH_3OH as a molecular probe.

(iv) The quantitative calorimetric data are in agreement with the data from the IR analysis (vide supra).

As a preliminary conclusion, beta-2 and beta-3 catalysts showed a distribution of acid sites of comparable strength, in line with Al content (as expected), although some influence of material morphology (especially zeolite crystal size), cannot be excluded.

Fig. 5 reports the differential heat of adsorption of H_2O vapour as a function of the increasing surface coverage (q^{diff} vs n_{ads}) for all of the catalysts investigated here. For comparison purposes, an Al-free beta-silicalite was added, along with a previously investigated [35,51] beta-10 sample, characterised by a much higher Al content (Si/Al ≈ 10), that is, a much greater number of Al atoms per unit cell (∼6; Table 1). The corresponding volumetric isotherms are shown in the inset. For brevity, in both q^{diff} versus n_{ads} and n_{ads} versus p_{eq} plots, only the first-run adsorption data are reported and discussed; however, in all catalysts, irrespective of Al content, a fraction of water molecules was irreversibly adsorbed, whereas for the beta-silicalite, the adsorption was completely reversible on outgassing at room temperature.

Our findings can be summarised as follows:

(i) Initially, the experimental data of q^{diff} versus coverage for beta-2 and beta-3 are best fitted by the same curve as for the CH_3OH q^{diff} versus n_{ads} plots (Fig. 4), partially confirming the close similarity of the acidic and hydrophilic properties of the two systems. However, the curve starts at $q_0 = 160$ kJ/mol for the two samples, but drops more rapidly for beta-3 than for beta-2, eventually approaching the latent heat of liquefaction of water ($q_L = 44$ kJ/mol) at a much lower coverage for beta-3 than for beta-2. Indeed, contrary to methanol, the H_2O absorption capacity of beta-3 is much lower than that for beta-2 (see the volumetric isotherms in the inset), indicating that although beta-3 has a slightly higher Al content than beta-2, it also has a lower population of sites active toward H_2O. In conclusion, beta-3 zeolite is less hydrophilic than beta-2 despite the lower Si/Al ratio, as if the larger crystal size of the former inhibits interaction with water.

(ii) The q_0 value (close to 100 kJ/mol) for the Na-rich beta-1 catalyst was much lower than those for beta-2 and beta-3, as expected. Furthermore, with increasing coverage, the beta-1 curve merged into the beta-2 curve, because of the close similarity in crystal size. It is noteworthy that the water adsorption capacity (per unit cell) of beta-1 was only slightly lower than that for beta-2 and much higher than that for beta-3, due to the lower concentration of strong acid sites (see the inset of Fig. 5).

(iii) The q^{diff} versus n_{ads} plot for beta-silicalite was below those of the other catalysts in the range of coverage examined, in agreement with the absence of strong acidic sites associated with framework Al species. The q_0 value for this sample was close to 80 kJ/mol, much lower than that for other zeolites. Note, however, that the q^{diff} versus n_{ads} plot for beta-silicalite was above the latent heat of liquefaction of water ($q_L = 44$ kJ/mol), as is typical of an hydrophilic surface [35–37].

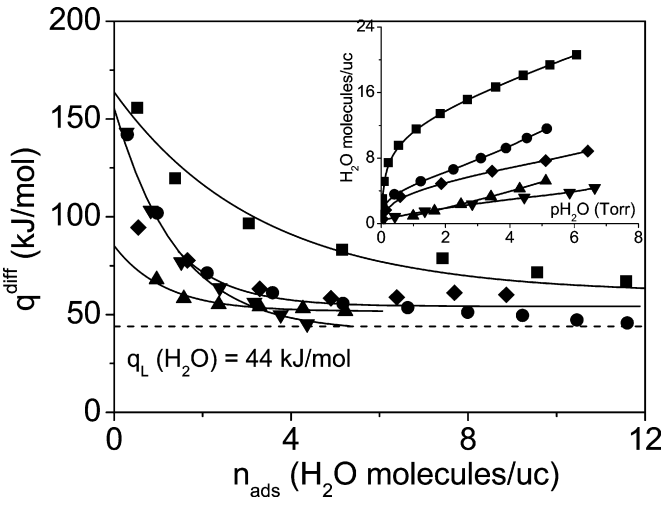

Fig. 5. Differential heats of adsorption of H_2O_{vap} on beta-1 (◆), beta-2 (●), beta-3 (▼) and beta-silicalite (▲), in comparison with catalyst beta-10 (■), characterised by Si/Al = 10. Inset: volumetric isotherms, n_{ads} (H_2O molecules/uc) vs p_{H_2O} equilibrium pressure. In both q^{diff} vs n_{ads} and n_{ads} vs p_{eq} plots only the first run data (ads. I) are reported. $T_{ads} = 303$ K.

Comparing the results for beta zeolites reported in the present study with those previously obtained for beta-10 makes the difference in calorimetric response of the Al-rich beta-10 system dramatically evident. Both the beta-10 q^{diff} versus n_{ads}

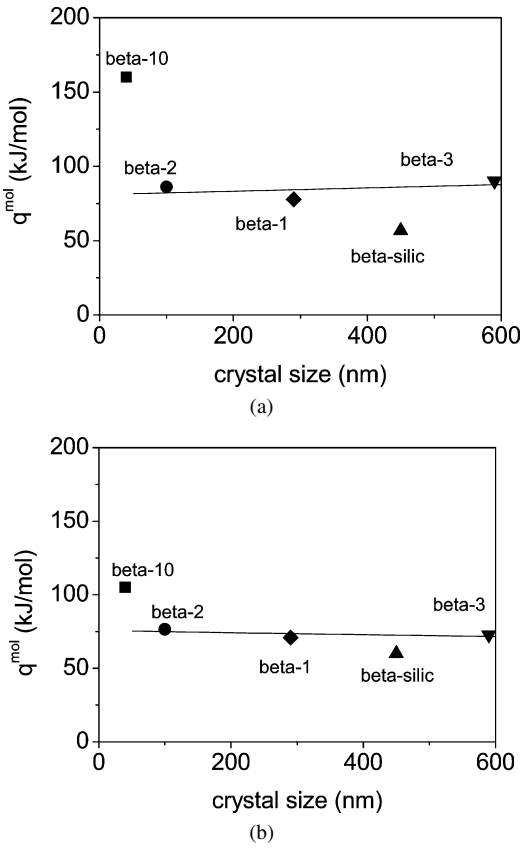

Fig. 6. Integral molar heats of adsorption $[q^{\mathrm{mol}}]_p = (Q^{\mathrm{int}}/n_{\mathrm{ads}})$ as a function of the average crystals size of the catalyst, at two different surface coverage: $n_{\mathrm{ads}} = 2$ H_2O molecules/uc (left) and $n_{\mathrm{ads}} = 4$ H_2O molecules/uc (right). $T_{\mathrm{ads}} = 303$ K.

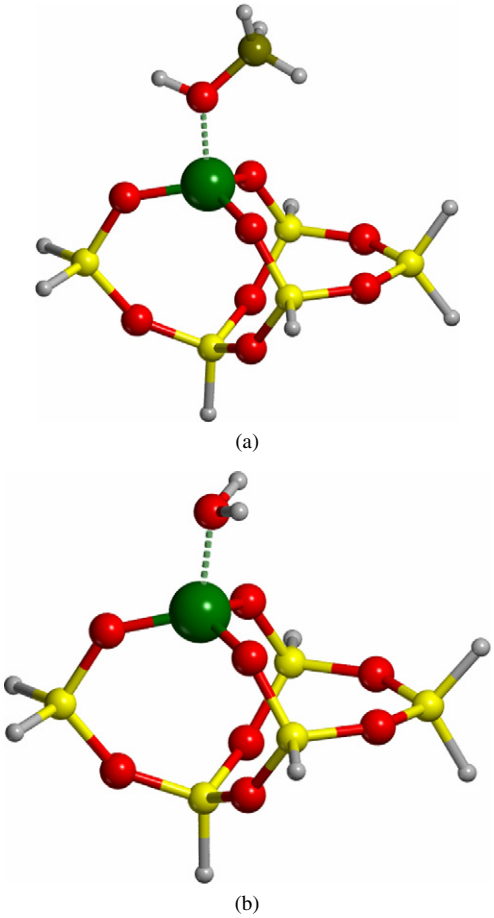

Fig. 7. B3LYP/6-31+G(d,p) optimized structures of the clusters adopted to mimic the Lewis site interacting with CH_3OH (a) and H_2O molecule (b). Binding energies (BE for (a) 125 and for (b) 110 kJ/mol) corrected for the basis set superposition error. Bonds between Al and the oxygen atom of the adsorbed molecule shown as dotted lines.

and n_{ads} versus p_{eq} plots lie well above the corresponding curves for the beta zeolites that we obtained. This strongly confirms that the population of strong acidic sites is much more abundant in the beta-10 catalyst, as expected. However, the initial heat of adsorption of water is quite close for the beta-2, beta-3, and beta-10 catalysts ($q_0 \sim 160$ kJ/mol in all cases), suggesting that the difference in calorimetric response is connected more to the abundance of acid site than to the strength of these sites.

The integral molar heat of adsorption q_{mol} (vide supra) determined at equilibrium pressure, corresponding to either 2 or 4 H_2O molecules/uc coverage, are shown in Figs. 6a and 6b as a function of the crystal size of the investigated materials (see Table 1). Again, data for beta-10 are reported for comparison. Our findings can be summarised as follows:

(i) The q_{mol} value was very close (∼85 kJ/mol, irrespective of the crystal size) for all catalysts, characterised by a close Si/Al ratio (130 < Si/Al < 154).

(ii) The q_{mol} value for beta-silicalite was lower (∼50 kJ/mol), due to the fact that in this case, only H-bonding interactions, much less energetic than both the Lewis and Brønsted acid–base interactions, were operative.

(iii) The q_{mol} value for beta-10 was much higher (∼160 kJ/mol), because the coverage of 2 H_2O molecules/unit cell was still very low, indicating that only one-third of the acidic sites associated with framework Al had reacted.

(iv) At a coverage of 4 H_2O molecules/unit cell over beta-10, a few strong acidic sites were available, but in this case the q_{mol} values (intrinsically average values, including all interaction contributions) were much closer (∼100 kJ/mol) to the q_{mol} values (∼75 kJ/mol) for the beta-1, -2, and -3 catalysts.

(v) At high coverage, the difference between the beta-1, -2, and -3 set and beta-silicalite was much smaller, due to the fact that at such coverage, the interaction was dominated by H-bonding on both silanols and already adsorbed water molecules in the beta-1, -2, and -3 catalysts as well.

Fig. 7 shows the B3LYP/6-31+G(d,p) optimized structures of the clusters adopted to mimic the Lewis acid site interacting with the CH_3OH (a) and H_2O (b) molecules. The calculated BEs were 125 and 110 kJ/mol, respectively. These values are in agreement with the calorimetric energetic data (differential heats of adsorption) measured in the early stage of the process and suggest that at least a fraction of acid sites are likely Lewis in nature.

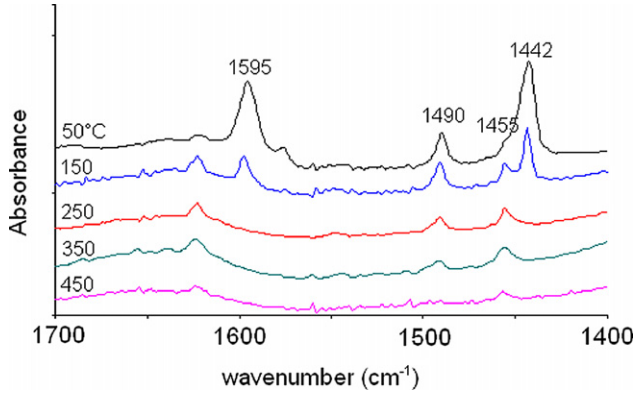

Fig. 8. FTIR spectra of beta-1 catalyst after saturation with pyridine followed by evacuation at progressively increasing temperature.

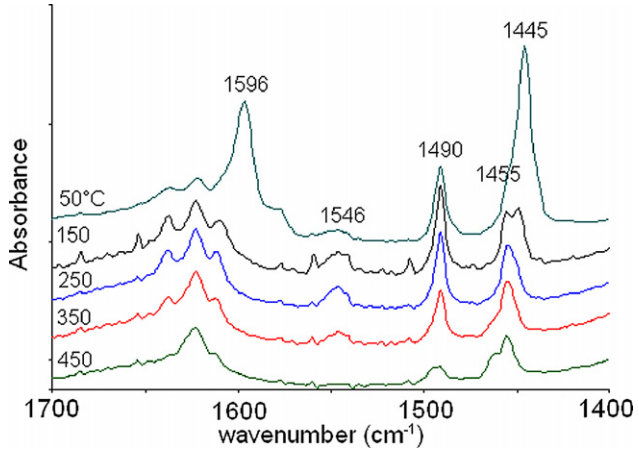

Fig. 9. FTIR spectra of beta-2 catalyst after saturation with pyridine followed by evacuation at progressively increasing temperature.

3.1.4. Nature and strength of surface acidity by FTIR of preadsorbed pyridine

Figs. 8 and 9 show the FTIR spectra recorded after pyridine adsorption at room temperature, followed by desorption at increasing temperatures, for the beta-1 and beta-2 samples, respectively. For beta-1 (Fig. 8), the intensity of the band associated with pyridinium cation (1546 cm^{-1}) was absent, that relative to the interaction with Lewis sites (1455 cm^{-1}) was very weak, and pyridine was released already after evacuation at 250 °C. Finally, the amount of pyridine interacting with silanols (bands at 1446 and 1596 cm^{-1}) [52] was lower than for beta-2 catalysts (Fig. 9). In beta-1, clearly silanols were the only sites present in nonnegligible amounts.

For beta-2 (Fig. 9), the strong bands at 1446 and 1596 cm^{-1}, due to pyridine adsorbed on silanols, decreased progressively with increasing temperature and totally disappeared after evacuation at 250 °C. In contrast, some pyridine adsorbed on Lewis sites (1455 cm^{-1}) remained even after evacuation at 450 °C. This indicates the presence of strong Lewis-type acid sites, in line with what was found by the other techniques. The band at 1546 cm^{-1}, due to the interaction with Brønsted sites, was very weak, as expected from the low concentration of these sites in high-silica zeolites. When the sample was heated, the intensity first increased (likely due to the evolution of the hydrogen bonding with the –OH group into pyridinium ions) and then decreased, totally disappearing after evacuation at 450 °C. The spectra recorded with beta-3 samples (not reported here for space considerations) were very similar to those recorded with beta-2 samples.

3.2. Catalyst activity and deactivation rate

There is a vast literature dealing with the use of zeolites as catalysts for the liquid-phase and gas-phase methylation of phenol. With MFI zeolites, at temperature above 350 °C, Kaliaguine et al. [2,53] found that this reaction led to various products, among which cresols and xylenols are the most relevant. A mechanism was proposed in which diphenyl ether and anisole (the two products of etherification) are the reaction intermediates and interact with Brønsted sites and carbonium ions to yield *C*-methylated products. The reaction pattern was confirmed by others [12], who also found that in liquid-phase methylation, anisole and cresols are primary products, and anisole undergoes a consecutive transformation to cresols.

With H-Y zeolites, at 200 °C and phenol conversion <15% *O*-alkylation was found to be quicker than *C*-alkylation (the two reactions were substantially parallel), with an *o*-/*p*-cresol molar ratio of 1.5. Anisole disproportioned into phenol- and methyl-anisoles, whereas direct isomerisation of anisole into cresols did not occur. Anisole also acted as an alkylating agent for phenol to yield cresols and methyl anisoles. The latter reaction was favoured over the disproportion of anisole in the presence of phenol [5]. An important contribution to *C*-alkylated compounds also derived from the intramolecular rearrangement of anisole into *o*-cresol [9]. The exchange of protons with Na or poisoning with NH_3 led to an increased anisole/cresols ratio, indicating that anisole formation requires sites with lower acid strength compared with those needed for cresol formation [6], in agreement with findings of Namba et al. [10]. Similar results were also obtained by other authors [7–9].

The reactivity of Al-MCM-41 also is similar to that of H-Y [39], with anisole acting as a reaction intermediate. The mechanism of reaction, involving direct formation of anisole and cresols and consecutive transformation of anisole, was recently confirmed by Weitkamp et al. [54] through in situ measurements.

With beta zeolites, again the formation of anisole and cresols occurred through parallel reactions [22,23]. Anisole was then the intermediate in the formation of cresols. As for the effect of the Si/Al ratio, higher ratios implied lower phenol conversion and hence greater selectivity to anisole. No effect of shape selectivity was found.

As for the electrophylic substitution on phenol, the active species is generated by adsorption of methanol and formation of framework-bound methoxonium ($CH_3OH_2^+$) ion and methoxy species, which can coexist at low temperature. However, at higher temperatures, the equilibrium shifts toward the methoxy species [55], which acts as an electrophylic alkylating agent on alkylaromatics [56,57].

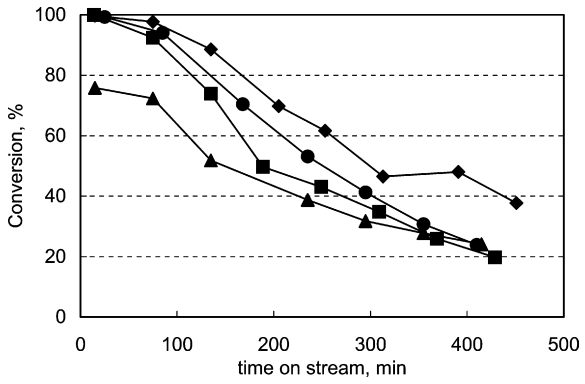

Fig. 10. Effect of time-on-stream on conversion of phenol in alkylation over beta-2 catalyst at four different temperatures: 320 (▲), 350 (■), 390 (◆) and 450 °C (●).

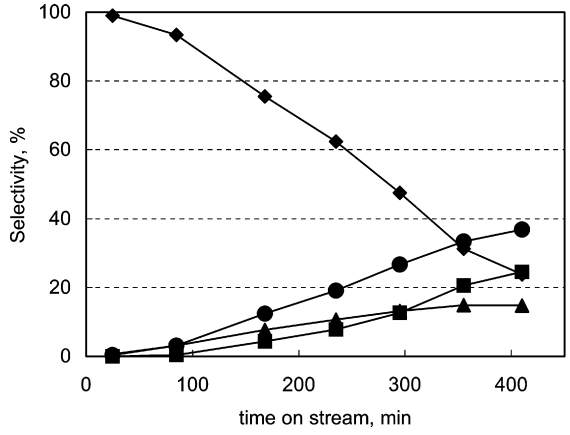

Fig. 11. Effect of time-on-stream on products distribution in alkylation of phenol over beta-2 catalyst. $T = 450\,^{\circ}C$. Selectivity to poly-alkylated phenol (◆), to *o*-cresol (●), to *p*-cresol (▲) and to anisole (■).

3.2.1. *Performance of beta-2 and beta-3 catalysts in phenol methylation*

Fig. 10 shows the effect of time on stream on conversion of phenol in methylation over the beta-2 catalyst at four different temperatures. Fig. 11 shows the corresponding distribution of products, measured at 450 °C. The following considerations are of relevance:

(i) Considerable catalyst deactivation occurred with increasing time on stream.
(ii) Initial conversion was 100% at temperatures above 320 °C and approached 75% at 320 °C.
(iii) The deactivation rate appears to be substantially independent of temperature.
(iv) Deactivation was accompanied by a change in the relative amount of products. Specifically, at total conversion, the main products were polyalkylated compounds (mainly di- and tri-methyl phenols and methyl and di-methyl anisoles), whereas the progressive decrease of conversion led to a rapid decrease of the latter compounds, with a corresponding increase in the primary alkylation products anisole, *o*-cresol, and *p*-cresol. Of these latter products, the most prevalent was *o*-cresol.
(v) A more detailed investigation of the trend of products formation indicated that the selectivity to cresols decreased monotonously with increasing conversion, whereas the selectivity to anisole decreased more rapidly. This is because the cresols underwent consecutive reactions of transformation to diphenols, whereas anisole not only underwent analogous consecutive alkylation to methyl anisole, but also acted as an alkylating agent by itself. Indeed, it is known that anisole can either rearrange to *o*-cresol (intramolecular rearrangement) or act as an intermolecular alkylating agent, with cogeneration of phenol [5,9,39,54].
(vi) At lower temperatures, the distribution of products was similar to that obtained at 450 °C. The only difference was in the selectivity ratio between anisole and cresols.

It is noteworthy that in the alkylation of alkylbenzenes (e.g., of toluene) with methanol, it is possible to obtain a high selectivity to the *para*-*C*-alkylated compound. In contrast, in the alkylation of activated arenes, such as phenol, diphenols and aniline, with olefins or with alcohols, the selectivity for the *para*-electrophilic substitution was lower than expected [58]. Indeed, on amorphous acid catalysts, the selectivity to *o*-cresol can even approach 100% [8,59,60]. The low selectivity to *p*-cresol in phenol methylation has been attributed to different factors [61,62], specifically the following:

(i) The alkylation at heteroatom is an intermediate step in *C*-alkylation by the olefin or the alcohol [63].
(ii) An interaction exists between the alkylating agent and the oxygen atom of phenol that favours alkylation at the *ortho* position [5,63].
(iii) A reaction between adsorbed anisole, which acts as the alkylating agent, and gas-phase phenol can be hypothesised [8] in which the interaction between the two O atoms puts the methyl group of anisole closer to the *ortho* position of phenol.
(iv) Furthermore, even in the homogeneous acid-catalysed electrophylic substitution on phenols, *ortho*/*para* ratios >2/1 are usually found [58,64]. This implies that adsorptive/geometric effects are not the main reasons for the regioselectivity observed here.

Consequently, the overall mechanism for the acid-catalysed methylation of phenol [8] includes direct *C*-alkylation at the *ortho* and *para* positions (in confined environments, direct *para*-*C*-alkylation may be preferred) and *O*-alkylation to yield anisole, with the ratio of *C*-/*O*-alkylation a function of the catalyst's acid strength. Thus, the present data on acidity, hydrophilicity/hydrofobicity, and energetics of the interaction with CH_3OH (vide supra) can help elucidate the role of different acid sites in both catalyst activity and deactivation. The secondary, consecutive intramolecular rearrangement of anisole to *o*-cresol makes the final *ortho*/*para* *C*-alkylation ratio very high, especially over less acidic catalysts (e.g., on amorphous materials).

The performance of the beta-3 catalyst is summarised in Fig. 12 (effect of time on stream on phenol conversion at four

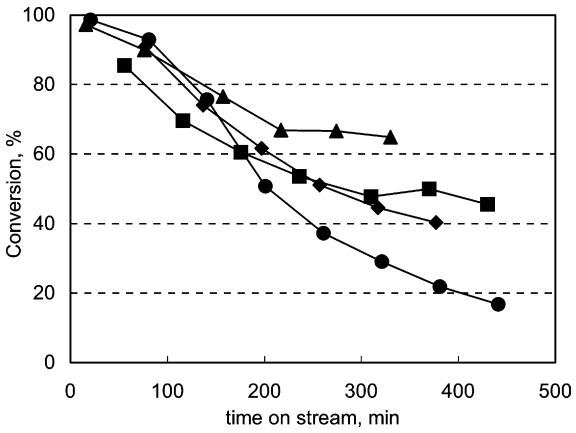

Fig. 12. Effect of time-on-stream on conversion of phenol in alkylation over beta-3 catalyst at four different temperatures. Symbols as for Fig. 10.

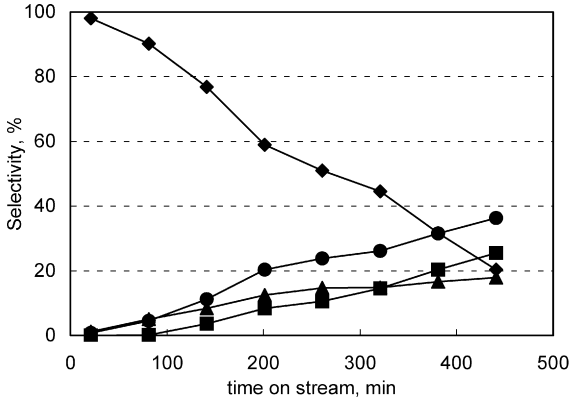

Fig. 13. Effect of time-on-stream on products distribution in alkylation of phenol over beta-3 catalyst. $T = 450\,^{\circ}C$. Symbols as for Fig. 11.

different temperatures) and Fig. 13 (effect of time on stream on distribution of reaction products at 450 °C). A comparison with the data obtained with the beta-2 zeolite (Figs. 10 and 11) reveals the following:

(i) The initial activity of the beta-3 zeolite was greater than that of beta-2. This was evident for the runs at 320 °C only; higher temperatures led to total or almost total conversion for both catalysts. This difference is very likely due to the higher intraparticle residence time of reactants in the larger-crystal size zeolite.

(ii) At higher temperatures, the deactivation rate seemed little affected by crystal size. Only at 320 and 350 °C did the beta-2 zeolite exhibit more rapid deactivation than beta-3. This likely was due to the shorter mean path within the smaller zeolite crystals, the pores of which became obstructed more quickly than the longer pores of beta-3. The fact that this difference was evident only at low temperatures indicates that the species responsible for deactivation are not the alkyl-aromatics formed by methanol transformation (the formation of which is favoured at high temperature), but more likely phenol and oxygenated products, the diffusion of which occurs more slowly at lower temperature, due to their low volatility and stronger interaction with the zeolite acid sites. The characterisation of spent catalysts (vide infra) confirms this hypothesis.

(iii) The nature of products and the effect of conversion and of temperature on selectivity did not differ significantly from those observed with the beta-2 catalyst.

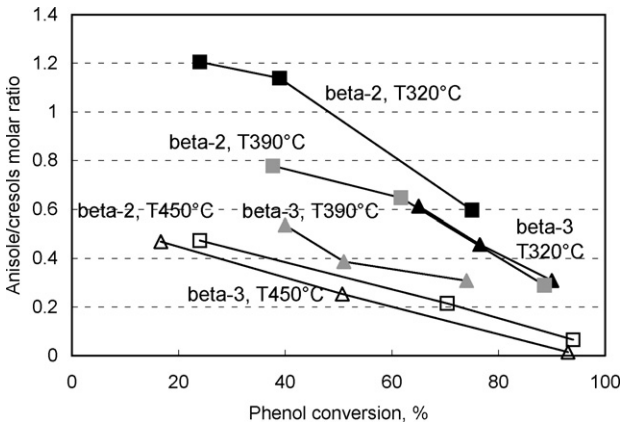

Fig. 14. Effect of phenol conversion on the anisole/cresols molar ratio at 320 °C (black symbols), 390 °C (grey symbols) and 450 °C (white symbols), for the beta-2 (squares) and beta-3 (triangles) catalysts.

Finally, Fig. 14 shows the effect of phenol conversion on the anisole/cresols ratio at 320, 390, and 450 °C on beta-2 and beta-3 catalysts. We can see that (i) the ratio decreased with increasing conversion, due to the secondary consecutive transformations occurring on anisole, with formation of additional cresols, and (ii) the ratio decreased with increasing temperature at any conversion level, indicating that low temperature favours primary methylation at oxygen (and hence to anisole) over primary methylation at aromatic carbons.

Even though the comparison between zeolites is debatable when done under conditions leading to catalyst deactivation and coke accumulation, the data of Fig. 14 indicate that the anisole/cresols ratio for beta-3 zeolite was systematically lower than that for beta-2 at any conversion level and any temperature. This means that the extent of the consecutive transformation of anisole to cresols was higher in the larger-crystal size zeolite, due to the longer permanence of anisole within the zeolite pores, favouring both the secondary consecutive intramolecular rearrangement and intermolecular alkylation of anisole.

An effect of crystal size on products distribution was also reported by Moon et al. for phenol methylation over MCM-22 [12]. Those authors found that *p*-cresol formed preferentially with respect to *o*-cresol, especially for catalysts with zeolite crystal size >1 μm. Consequently, they proposed that for MCM-22, the 10 MR pores allow easy diffusion of *p*-cresol, and that the effect of this phenomenon is enhanced when the crystal size is relatively large. In the case of cresol isomerisation, the distribution of isomers (the formation of which occurs both by intramolecular methyl shift and bimolecular disproportionation) is governed by product desorption/diffusion. Shape selectivity favours monomolecular reactions [65].

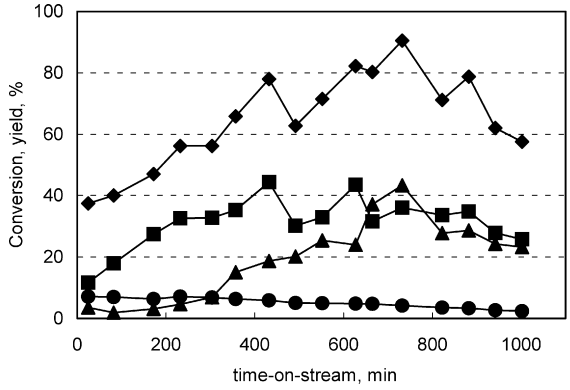

Fig. 15. Effect of time-on-stream on methanol conversion and on products distribution in polyalkylbenzenes formation over beta-2 catalyst. $T = 390\,^{\circ}C$. Symbols: (◆) methanol conversion; (●) selectivity to toluene, (■) to pentamethylbenzene, (▲) to hexamethylbenzene.

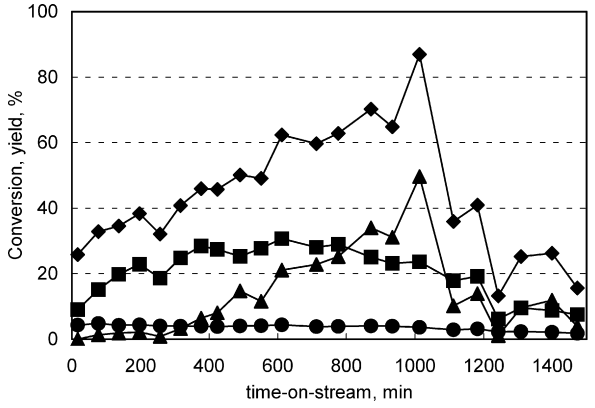

Fig. 16. Effect of time-on-stream on methanol conversion and on products distribution in polyalkylbenzenes formation over beta-3 catalyst. $T = 390\,^{\circ}C$. Symbols as for Fig. 15.

3.2.2. *Transformation of methanol into polyalkylated benzenes*

During reaction with phenol, methanol also undergoes a parallel transformation to olefins and alkylbenzenes. The relative amounts of the two classes of compounds are a function of reaction temperature, with higher temperatures favouring the formation of the latter compounds. Therefore, we also investigated the formation of alkylbenzenes. Figs. 15 and 16 show the yields of these compounds for the beta-2 and beta-3 catalysts, respectively, as a function of time on stream at 390 °C in tests performed by feeding only methanol. It noteworthy that no "light" products of methanol decomposition (i.e., CO, CO_2, or H_2) was formed.

The principal products coming from methanol transformation were toluene, pentamethylbenzene, and hexamethylbenzene. Minor byproducts were xylenes and tri- and tetra-methyl benzenes. The present paper is the first report of this finding in the literature on gas-phase methylation of phenol catalysed by zeolites. Furthermore, it is evident that this is one reason for the need to feed a large excess of methanol with respect to the stoichiometric requirement for mono-alkylation. The competitive reaction of methanol transformation to alkylbenzenes significantly decreases the amount of methanol available for phenol methylation.

The conversion of methanol increased during the elapsing reaction time, due to the increased formation of polyalkylated compounds. Therefore, it seems that the active sites for the formation of these compounds were generated during reaction. The conversion of methanol reached a maximum at approximately 800–1000 min on stream, after which it dropped rapidly, likely due to the considerable amount of coke accumulated in the catalyst from the growth of polynuclear aromatics. Polyalkylbenzene formation was also observed during the reaction of phenol methylation; however, in this case the yields of these compounds were lower than those found in the absence of phenol.

The behaviour of the two zeolites did not differ much, apart from the slightly different value of time on stream at which the maximum methanol conversion was attained (700 min for beta-2 vs 1000 min for beta-3). This is probably due to the larger crystal size of the latter sample, which increased the time for pore filling by coke compared with that in the former sample. With both samples, the yield to toluene decreased, whereas that to pentamethylbenzene showed a maximum before the reaction time needed to reach the highest methanol conversion. The yield to the totally alkylated compound (hexamethylbenzene) increased until the maximum methanol conversion was reached, indicating that growth of the molecular weight occurred in a consecutive-steps network fashion.

The formation of alkylated benzenes by self-reaction of methanol over zeolites (the MTG process) includes a first step of dehydration of methanol to dimethylether. Two mechanisms for this have been proposed: an indirect pathway, in which the adsorbed methanol reacts with the methoxy species, which then reacts with another methanol molecule to dimethylether [66], and a direct pathway, in which two methanol molecules react over an acid site, with the formation of dimethylether and H_2O in a single step [67]. The surface methoxy species $SiO(CH_3)Al$ plays a role in the formation of dimethylether [68]. The further conversion of the equilibrium mixture of methanol and dimethylether (as well as water) is dominated by a "hydrocarbon pool" route [69,70] in which methanol is directly added onto reactive organic compounds to form aliphatic and aromatic hydrocarbons. The methoxy species also plays a role in the kinetic "induction period," leading to the reactive hydrocarbon pool.

Alternative "direct" mechanisms have been proposed in which a carbenium ion (CH_3^+) reacts with dimethylether to generate either a carbonium ion (CH_3–CH_3^+–OCH_3) or an oxonium ylide species. Other mechanisms include a carbene species ($:CH_2$) as the reaction intermediate; see the review by Haw et al. [71] for an analysis of the several mechanisms proposed in the literature. The methoxy species acts as an alkylating agent in the presence of aromatic compounds. Furthermore, at $T > 170\,^{\circ}C$, hydrogen atoms are abstracted by basic oxygen atoms of the framework, with formation of surface-stabilised intermediates of a ylide or carbene nature [72], which are responsible for the methylation of aliphatic compounds and the formation of hydrocarbons, both aliphatic and aromatic (polymethylbenzenes) [73].

In the case of beta zeolites, the predominant aromatic compounds in methanol transformation at high temperature were hexamethylbenzenes and pentamethylbenzenes (in full agreement with our results), whereas ZSM-5 gave mostly dimethyl and trimethylbenzenes [74]. These compounds can be further converted to naphthalene derivatives, which are finally responsible for the formation of coke precursors and of zeolite deactivation [21].

Our data support the need for an induction period for the formation of these compounds, associated with the generation of a "hydrocarbon pool." This corresponds to the progressive increase of methanol transformation into polyalkylbenzenes shown in Figs. 15 and 16. The progressive transformation of the hydrocarbon pool into increasingly heavier polyalkylated compounds and to coke leads eventually to complete deactivation of the catalyst.

3.2.3. Coke composition

Thermogravimetric (TG) analysis showed a weight loss due to burning out of coke components trapped in aged catalyst by calcination in air of 3.4% for beta-1 and 12.8% for beta-2. These findings obviously relate to the higher acidity of beta-2 compared with beta-1. The organic matter extracted from beta-2 with CH_2Cl_2 amounted to 12.7%, perfectly in line with the value determined by TG. GC-QMS analysis of the extracted fraction showed the presence of the following compounds: phenol (8 mol%), *o*- and *p*-cresols (4%), dimethylphenols (8%), trimethylphenols (15%), tetramethylphenols (18%), pentamethylbenzene (5%), hexamethylbenzene (5%), 3-ethyl-5-methylphenol (1%), 2-hydroxyphenyl-phenylmethanone (15%), 2-methyl-5-(1-methylethyl)-phenol (6%), and 1-methoxy-4-methyl-2-(1-methylethyl)-benzene (15%). In the case of beta-1, the following compounds were identified: phenol, cresols, dimethylphenols, trimethylphenols, tetramethylphenols, and (dimethyl-ethyl)-phenols. Thus, for beta-1 there was substantially no formation of polyalkylbenzenes—the species coming from the transformation of methanol. With both catalysts, the insoluble coke recovered after dissolution of the zeolite was almost weightless and presumably composed of high-molecular-weight polynuclear species; their very low amount prevented any reliable quantitative determination, however.

These data indicate that the presence of strong Lewis acid sites in beta-2 is responsible for the formation of polyalkylbenzenes, whereas silanols (present in both the beta-1 and beta-2 samples, though in a lower concentration in the former) are strong enough to catalyse the reaction of phenol methylation. This also indicates that the active methanol species able to attack phenol to yield methylated phenol is different from the species that self-reacts to yield polyalkylbenzenes. Indeed, on one hand, the latter species can form only on acid sites much stronger than those needed to form the former species, but on the other hand, the former species, although not able to generate polyalkylbenzenes, is sufficiently electrophylic to react with phenol.

Furthermore, beta-1 was less active than beta-2 and beta-3 (data not reported), but exhibited a comparable deactivation rate. This indicates that the main reason for catalyst deactivation in phenol methylation is associated with the build-up of oxygen-containing species (phenol and alkylated phenol compounds) in catalyst pores. It is noteworthy that analysis of the compounds retained in the pores revealed a high concentration of heavier species (polyalkylated phenol) that instead are present in low concentrations in the reactors' outgoing product stream. Therefore, heavier phenol derivatives accumulate more easily in the porous structure, as expected due to their more cumbersome structure.

Consequently, two different deactivation mechanisms can be envisaged. One mechanism responsible for the progressive deactivation of the catalyst in the methylation of phenol is due to the retention of heavy, oxygenated compounds (i.e., polyalkylated phenols). These compounds are derived from the strong interaction of phenol and phenol derivatives with the active sites, which is established from the very beginning of the reaction and hinders generation of the active species responsible for the electrophylic attack on the phenol aromatic ring. Methanol is simultaneously converted to alkyl and polyalkylbenzenes, generated from the buildup of the "hydrocarbon pool" inside pores. This mechanism is also supported by the change in the nature of the alkylbenzenes forming along with increasing methanol conversion. However, the progressive hardening of these species generates polynuclear aromatics, which fill up the pores within a few hours and eventually deactivate the catalyst.

4. Conclusions

The systematic analysis carried out in the present work provided insight into several aspects of the methylation of phenol from various points of view, ranging from catalyst structure, crystal size, and surface acidity characteristics, to the energetics of the interaction between methanol and water and acid sites and the effect of all of these characteristics on the kinetics and mechanistic features of the catalytic reaction and catalyst deactivation phenomena. The main conclusions that can be drawn from our results can be summarised as follows:

1. High Si/Al ratio BETA-structured zeolite in protonated form is a very active catalyst for the methylation of phenol, leading to cresols and anisole as primary products, which rapidly methylate to polyalkylated phenols. As catalyst deactivation proceeds, the selectivity to cresols and anisole increases significantly, and the selectivity to polyalkylated species decreases rapidly.
2. In this protonated zeolite, acidity is predominately of the Brønsted type, independent of zeolite crystal size. The acid sites are mainly of medium to low strength. High-strength Lewis-type sites either are almost absent (especially when metal cations are partially substituted for protons) or seem to play a role in catalyst deactivation.
3. Stacking faults in the zeolite framework, generated by the intergrowth of at least two BETA polymorphs, can increase the concentration of relatively low-strength silanol-based

acid sites. Nonetheless, these sites appear to be sufficiently active to trigger the phenol methylation primary reaction.

4. Deactivation is triggered essentially by phenol and polyalkylated phenol derivatives. Self-oligomerisation–cyclisation of methanol to olefins and aromatics, followed by further alkylation to aromatic C atoms, also contributes to catalyst deactivation.
5. At higher temperatures, all of the zeolites deactivate at a comparable rate, whereas at lower temperatures, initial catalytic activity is higher for larger-crystal size zeolites, due to the longer diffusion time of reactants within zeolite pores, favouring a longer contact time with active sites.
6. At any conversion level and any temperature, the anisole/cresols ratio is systematically lower for the larger-crystal size zeolites, because the secondary transformations of anisole to cresols by both intramolecular rearrangement and intermolecular alkylation of phenol is favoured by the longer residence time of anisole within the zeolite pores.

Acknowledgments

The financial aid of INSTM, through the Prisma 2002 programme is gratefully acknowledged. We are also indebted with dr A. Casalini, Stazione Sperimentale per i Combustibili (S. Donato Milanese) for the GC-QMS analysis of coke and with Polimeri Europa srl, Novara, for kindly supplying the beta-10 catalyst sample.

References

[1] Ullmann's Encyclopedia of Industrial Chemistry, vol. 9, sixth ed., Wiley–VCH, Weinheim, 2003, p. 642.
[2] P.D. Chantal, S. Kaliaguine, J.L. Grandmaison, Appl. Catal. 18 (1985) 133.
[3] R. Pierantozzi, A.F. Nordquist, Appl. Catal. 21 (1986) 263.
[4] S.C. Lee, S.W. Lee, K.S. Kim, T.J. Lee, D.H. Kim, J. Chang Kim, Catal. Today 44 (1998) 253.
[5] M. Marczewski, J.-P. Bodibo, G. Perot, M. Guisnet, J. Mol. Catal. 50 (1989) 211.
[6] L. Garcia, G. Giannetto, M.R. Goldwasser, M. Guisnet, P. Magnoux, Catal. Lett. 37 (1996) 121.
[7] S. Balsamà, P. Beltrame, P.L. Beltrame, P. Carniti, L. Forni, G. Zuretti, Appl. Catal. 13 (1984) 161.
[8] P. Beltrame, P.L. Beltrame, P. Carniti, A. Castelli, L. Forni, Appl. Catal. 29 (1987) 327.
[9] R.F. Parton, J.M. Jacobs, H. van Ooteghem, P.A. Jacobs, Stud. Surf. Sci. Catal. 46 (1989) 211.
[10] S. Namba, T. Yashima, Y. Itaba, N. Hara, Stud. Surf. Sci. Catal. 5 (1980) 105.
[11] Z.-H. Fu, Y. Ono, Catal. Lett. 21 (1993) 43.
[12] G. Moon, W. Böhringer, C.T. O'Connor, Catal. Today 97 (2004) 291.
[13] M.D. Romero, G. Ovejero, A. Rodriguez, J.M. Gomez, I. Agueda, Ind. Eng. Chem. Res. 43 (2004) 8194.
[14] G. Sarala Devi, D. Giridhar, B.M. Reddy, J. Mol. Catal. 181 (2002) 173.
[15] F.M. Bautista, J.M. Campelo, A. Garcia, D. Luna, J.M. Marinas, A. Romero, J.A. Navio, M. Macias, Appl. Catal. A 99 (1993) 161.
[16] R. Bal, B.B. Tope, S. Sivasanker, J. Mol. Catal. A 181 (2002) 161.
[17] S. Velu, C.S. Swamy, Appl. Catal. A 145 (1996) 141.
[18] V.V. Rao, V. Durgakumari, S. Narayanan, Appl. Catal. 49 (1989) 165.
[19] S. Velu, C.S. Swamy, Appl. Catal. A 162 (1997) 81.
[20] M. Bolognini, F. Cavani, D. Scagliarini, C. Flego, C. Perego, M. Saba, Catal. Today 75 (2002) 103.
[21] M. Bjørgen, U. Olsbye, S. Kolboe, J. Catal. 215 (2003) 30.
[22] J. Xu, A.-Z. Yan, Q.-H. Xu, React. Kinet. Catal. Lett. 62 (1997) 71.
[23] G. Chen, X. Liu, Chin. J. Catal. 19 (1998) 427.
[24] K.K. Cheralathan, I.S. Kumar, M. Palanichamy, V. Murugesan, Appl. Catal. A 241 (2003) 247.
[25] A.V. Krishnan, K. Ojha, N.C. Pradhan, Org. Proc. Res. Dev. 6 (2002) 132.
[26] K. Zhang, C. Huang, H. Zhang, S. Xiang, S. Liu, D. Xu, H. Li, Appl. Catal. A 166 (1998) 89.
[27] E. Dumitriu, V. Hulea, J. Catal. 218 (2003) 249.
[28] I. Kiricsi, C. Flego, G. Pazzuconi, W.O. Parker Jr., R. Millini, C. Perego, G. Bellussi, J. Phys. Chem. 98 (1994) 4627.
[29] G. Bellussi, G. Pazzuconi, C. Perego, G. Girotti, G. Terzoni, J. Catal. 157 (1995) 227.
[30] G. Perego, S. Amarilli, R. Millini, G. Bellussi, G. Girotti, G. Terzoni, Mesoporous Mater. 6 (1996) 395.
[31] G. Girotti, EurpaCat-IV, Rimini, September 5–10, 1997, Book of Abstracts, KN11.
[32] J. Pérez-Pariente, J.A. Martens, P.A. Jacobs, Appl. Catal. 31 (1987) 35.
[33] M.A. Camblor, J. Pérez-Pariente, Zeolites 11 (1991) 202.
[34] U.S. Patent 5,453,511 (September 26, 1995).
[35] V. Bolis, B. Fubini, L. Marchese, G. Martra, D. Costa, J. Chem. Soc. Faraday Trans. 87 (1991) 497.
[36] V. Bolis, A. Cavenago, B. Fubini, Langmuir 13 (1997) 895.
[37] V. Bolis, C. Busco, S. Bordiga, P. Ugliengo, C. Lamberti, A. Zecchina, Appl. Surf. Sci. 196 (2002) 56.
[38] V. Bolis, C. Busco, P. Ugliengo, J. Phys. Chem. B 110 (2006) 14,849.
[39] K.G. Bhattacharyya, A.K. Talukdar, P. Das, S. Sivasanker, J. Mol. Catal. A 197 (2003) 255.
[40] P. Magnoux, P. Roger, C. Canaff, V. Fouché, N.S. Gnep, M. Guisnet, Stud. Surf. Sci. Catal. 34 (1987) 317.
[41] R.L. Wadlinger, G.T. Kerr, E.J. Rosinski, U.S. Patent 3,308,069 (1967) and reissued U.S. Pat. Re 28,431 (1975), assigned to Mobil Oil Corp.
[42] J.M. Newsam, M.M.J. Treacy, W.T. Koetsier, C. De Gruyter, Proc. R. Soc. London A 420 (1988) 375.
[43] J.B. Higgins, R.B. La Pierre, J.L. Schlenker, A.C. Rohrman, J.D. Wood, G.T. Kerr, W.J. Rohrbaugh, Zeolites 8 (1988) 446.
[44] C. Pazè, S. Bordiga, C. Lamberti, M. Salvalaggio, A. Zecchina, J. Phys. Chem. B 101 (1997) 4740.
[45] A. Zecchina, S. Bordiga, G. Spoto, D. Scarano, G. Spanò, F. Geobaldo, J. Chem. Soc. Faraday Trans. 9 (1996) 4863.
[46] S. Bordiga, L. Regli, D. Cocina, C. Lamberti, C.M. Bjørgen, K.P. Lillerud, J. Phys. Chem. B 109 (2005) 2779.
[47] G. Herzberg, Molecular Spectra and Molecular Structure, F.R.S., Infrared and Raman Spectra of Polyatomic Molecules, vol. II, D. Van Nostrand Company, Inc., New York, 1945, p. 216.
[48] S.E. Odinokov, A.V. Jogansen, Spetrochim. Acta Part A 28 (1972) 2343.
[49] N.B. Coltup, L.H. Daly, S.E. Wiberley, Introduction to Infrared and Raman Spectroscopy, Academic Press, London, 1995, p. 220.
[50] S.F. Boys, F. Bernardi, Mol. Phys. (1970) 553.
[51] V. Bolis, M. Broyer, A. Barbaglia, C. Busco, G.M. Foddanu, P. Ugliengo, J. Mol. Catal. A Chem. 204 (2003) 561.
[52] G. Busca, Phys. Chem. Chem. Phys. 1 (1999) 723.
[53] M. Renaud, P.D. Chantal, S. Kaliaguine, Can. J. Chem. Eng. 64 (1986) 787.
[54] W. Wang, P.L. De Cola, R. Glaeser, I.I. Ivanova, J. Weitkamp, M. Hunger, Catal. Lett. 94 (2004) 119.
[55] J. Rakoczy, T. Romotowski, Zeolites 13 (1993) 256.
[56] G. Mirth, J. Lercher, J. Catal. 132 (1991) 244.
[57] A. Corma, G. Sastre, P.M. Viruela, J. Mol. Catal. A 100 (1995) 75.
[58] R.F. Parton, J.M. Jacobs, D.R. Huybrechts, P.A. Jacobs, Stud. Surf. Sci. Catal. 46 (1989) 163, and references therein.
[59] J.M. Campelo, A. Garcia, D. Luna, J.M. Marinas, M.S. Moreno, Stud. Surf. Sci. Catal. 41 (1988) 249.
[60] J.M. Campelo, A. Garcia, D. Luna, J.M. Marinas, M.S. Moreno, Bull. Soc. Chim. Fr. 2 (1988) 283.
[61] P. Espeel, R. Parton, H. Toufar, J. Martens, W. Hölderich, P. Jacobs, in: J. Weitkamp, L. Puppe (Eds.), Catalysis and Zeolites. Fundamentals and Applications, Springer, Berlin, 1999, chap. 6, p. 377.

[62] J.B. Moffat, Catal. Rev. Sci. Eng. 18 (1978) 199.
[63] M. Marczewski, G. Perot, M. Guisnet, Stud. Surf. Sci. Catal. 41 (1988) 273.
[64] Patai, The Chemistry of the Hydroxyl Group, Interscience–Wiley, New York, 1971, p. 414.
[65] F.E. Imbert, M. Guisnet, F. Gnep, J. Catal. 195 (2000) 279.
[66] T.R. Forester, R.F. Howe, J. Am. Chem. Soc. 109 (1987) 5076.
[67] J. Bandiera, C. Naccache, Appl. Catal. 69 (1991) 139.
[68] W. Wang, M. Seiler, M. Hunger, J. Phys. Chem. B 105 (2001) 12553.
[69] I.M. Dahl, S. Kolboe, J. Catal. 149 (1994) 458.
[70] B. Arstad, S. Kolboe, J. Am. Chem. Soc. 123 (2001) 8137.
[71] J.F. Haw, W. Song, D.M. Marcus, J.B. Nicholas, Acc. Chem. Res. 26 (2003) 317.
[72] P.E. Sinclair, C.R.A. Catlow, J. Phys. Chem. B 101 (1997) 295.
[73] W. Wang, A. Buchholz, M. Seiler, M. Hunger, J. Am. Chem. Soc. 125 (2003) 15260.
[74] Ø. Mikkelsen, S. Kolboe, Microporous Mesoporous Mater. 29 (1999) 173.